Self-Learning e-Skin Respirometer for Pulmonary Disease Detection

Anand Babu, Getnet Kassahun, Isabelle Dufour, Dipankar Mandal, Damien Thuau

ADVANCED SENSOR RESEARCH Open Access
www.advsensorres.com

Self-Learning e-Skin Respirometer for Pulmonary Disease Detection

Anand Babu, Getnet Kassahun, Isabelle Dufour, Dipankar Mandal,* and Damien Thuau**

Amid the landscape of respiratory health, lung disorders stand out as the primary contributors to pulmonary intricacies and respiratory diseases. Timely precautions through accurate diagnosis hold the key to mitigating their impact. Nevertheless, the existing conventional methods of lungs monitoring exhibit limitations due to bulky instruments, intrusive techniques, manual data recording, and discomfort in continuous measurements. In this context, an unintrusive organic wearable piezoelectric electronic-skin respirometer (eSR) exhibiting a high-sensitivity (385 mV N^{-1}), precise conversion factor (12 mL mV^{-1}), high signal-to-noise ratio (58 dB), and a low limit of detection down to 100 mL is demonstrated, which is perfectly suitable to record diverse breathing signals. To empower the eSR with early diagnosis functionality, self-learning capability is further added by integrating the respirometer with the machine learning algorithms. Among various tested algorithms, gradient boosting regression emerges as the most suitable, leveraging sequential model refinement to achieve an accuracy exceeding 95% in detection of chronic obstructive pulmonary diseases (COPD). From conception to validation, the approach not only provides an alternative pathway for tracking the progression of lung diseases but also has the capability to replace the conventional techniques, with the conformable AI-empowered respirometer.

1. Introduction

Breathing is a fundamental aspect of respiratory physiology that provides vital information on pulmonary symptoms aiding in the assessment of chronic obstructive pulmonary diseases (COPDs) and other lung disorders.[1–3] Accurate measurement and surveillance of breathing features is challenging, due to the bulky nature and limited accessibility of conventional equipment such as spirometry, peak flow meter, body plethysmography, and gas diffusion tests to name a few. Moreover, these equipment need trained personals, specialized techniques, manual data recording, and dedicated testing facilities.[4–6] The invasive and cumbersome aspects of some of the techniques also limit their practicality in certain conditions, including continuous long-term monitoring during physical activities.[7–11] In contrast, the recent advancement in wearable sensor technologies have opened new possibilities for capturing physiological signals in a non-invasive and unobtrusive manner. Screen printing stands out as one of the promising techniques for printing the adaptable electronic-skin (e-skin), with its versatility, scalability, and customizability that offers precise deposition of functional materials onto different surfaces. On the contrary to other fabrication techniques, screen printing technologies allow printed sensors that are lightweight, flexible, and can be easily integrated into garments facilitating continuous monitoring in daily life activities.[12–14] Incorporating self-powered materials (such as piezoelectric materials) into printing processes adds a noteworthy advantage as comparison to their counterparts like capacitive and piezoresistive materials, which necessitate external biasing for operation.

Noteworthy to mention, the accurate measurement of breathing features such as tidal volume, inspiration capacity (IC), and forced expiratory volume in 1 s (FEV1), aids in the diagnosis and monitoring of progressive respiratory disorders and lung diseases, such as COPDs, asthma, idiopathic pulmonary fibrosis (IPF), and others.[15,16] For instance, reduced tidal volume is indicative of impaired lung function or respiratory muscle weakness, while, elevated tidal volume gives information about hyperinflation or increased work of breathing. Similarly, reduced IC and FEV1 values probed the presence of COPDs, signaling airflow limitation, airway obstruction, and emphysematous

A. Babu, G. Kassahun, I. Dufour, D. Thuau
Univ. Bordeaux
CNRS
INP
IMS
UMR 5218, Talence, Bordeaux F-33400, France
E-mail: anand.ph19217@inst.ac.in; damien.thuau@ims-bordeaux.fr
A. Babu, D. Mandal
Quantum Materials and Devices Unit
Institute of Nano Science and Technology
Knowledge City, Sector 81, Mohali 140306, India
E-mail: dmandal@inst.ac.in

The ORCID identification number(s) for the author(s) of this article can be found under https://doi.org/10.1002/adsr.202400079

DOI: 10.1002/adsr.202400079

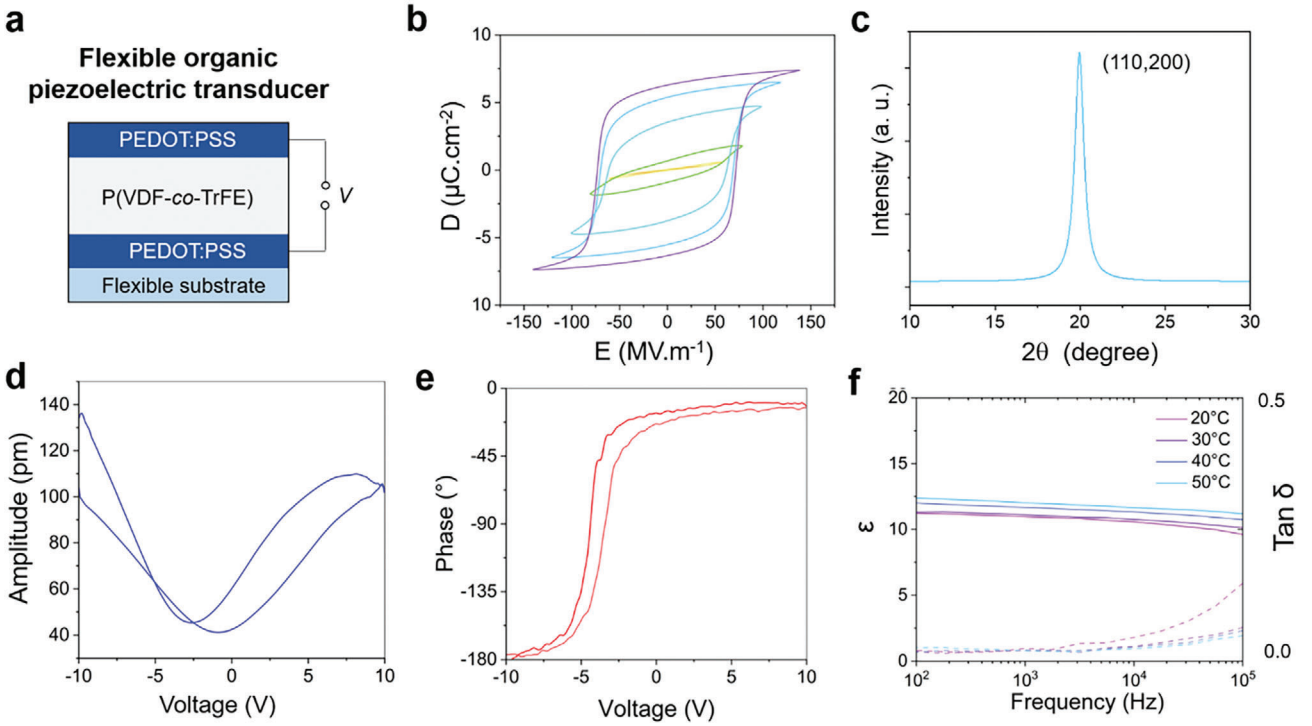

Figure 1. a) Cross section view is depicted in schematic illustration of our piezoelectric printed organic transducer. b) Electric displacement—electric field (D,E) loops. c) XRD pattern in the 2θ range [10°, 30°] of P(VDF-co-TrFE) copolymer measured at room temperature; d) PFM amplitude and e) phase loop of P(VDF-co-TrFE). f) Frequency and temperature-dependent dielectric constant and loss of P(VDF-co-TrFE).

changes. These parameters not only serve as diagnostic and prognostic markers but also guide personalized treatment strategies, highlighting their critical role in managing respiratory diseases and its progressive nature. Early detection of these biomarkers can enable timely interventions and better disease management.[17–21] In addition to disease detection, in the realm of sports and exercise physiology, these biomarkers serve as an essential metric for evaluating aerobic capacity, and exercise performance, providing insights into breathing patterns during physical activities.[22,23] Integrating self-learning capabilities into systems involves the utilization of machine learning (ML) algorithms. These algorithms operate on data driven techniques, leveraging data analysis to make informed decisions and identify unknown samples. For instance, the algorithms detect anomalies in biomarkers through learning process, enabling it to track the progression of diseases effectively.[24–29]

In this study, we demonstrate a ML integrated organic eSR able to record diverse breathing signals. A self-learning functionality has been added by harnessing the potent breathing descriptors with ML. A comprehensive study is carried out to find the most suitable prediction algorithms including random forest regression (RFR), gradient boost regression (GBR), linear regression (LR), support vector machines (SVM), and ridge regression (RR), among them GBR was found to be the most effective one with accuracy over 95% and root mean square error 0.298. Thus, eSR provides a non-invasive and practical solution for tracking and early prediction of progressive lung diseases that helps to take the diagnosis measures in early stage for personalized disease management.

2. Results and Discussion

To capture precise respiratory signals, piezoelectric eSRs are fabricated using a sequential screen-printing process, which involves layering poly(3,4-ethylenedioxythiophene)-poly(styrenesulfonate) (PEDOT: PSS) as the bottom electrode, polyvinylidene fluoride trifluoroethylene (P(VDF-*co*-TrFE)) as the electroactive material, and (PEDOT: PSS) as the top electrode onto a flexible polyethylene naphthalate (PEN) substrate, as depicted in **Figure 1a**. Polarization of the P(VDF-*co*-TrFE) thin film is accomplished by applying an electric field across the PEDOT:PSS electrodes deposited on outer surfaces. Electric displacement–electric field (D,E) loops are recorded with a TF Analyzer 2000 (aixACCT System) at 300 K (Figure 1b), where increasing the applied electric field resulted in a systematic increase in the remnant polarization (P_r). Well-saturated hysteresis loops are obtained at 150 MV m^{-1}. The typical P_r and coercive field (E_c) values are found 6.2 μC cm^{-2} and 67 MV m^{-1}, respectively, indicating that the polymer can sustain an electric field as high as 150 MV m^{-1}. To further ensure the good quality of the printed P(VDF-*co*-TrFE) copolymer, XRD characterization is carried out, and displays a diffraction peak at $2\theta = 20.0°$, which corresponds to an interchain lattice spacing of 4.439 Å (calculated from Bragg's equation $2d \sin\theta = n\lambda$) from the (110, 200) reflection in ferroelectric crystalline phases (Figure 1c). At the nanoscale, local switching piezoelectric measurements, and piezoresponse force microscopy (PFM) are employed to track the polarization switching corresponding to the applied voltage in a direction perpendicular to the substrate. The P(VDF-*co*-TrFE)

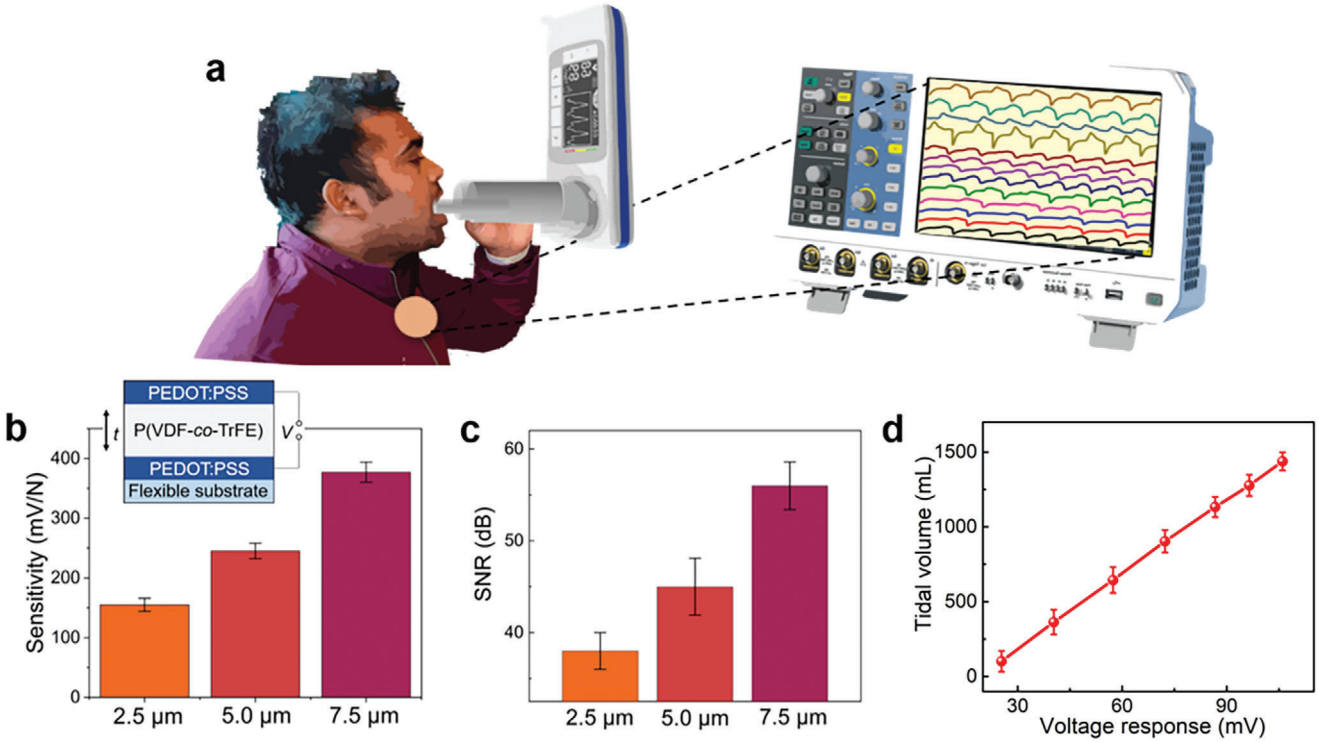

Figure 2. a) Schematic illustrating the calibration process of eSR for detection of tidal volume. b) Sensitivity measurement and c) Signal-to-noise ratio (SNR) at a constant force for eSRs with varying thicknesses of P(VDF-co-TrFE) d) Calibration plot of tidal volume measurement with the eSR.

thin films represent polarization switching pertaining to the piezo-ferro-electric behavior as shown by the butterfly loop behavior of PFM amplitude and the presence of a large hysteresis in the phase versus DC voltage is shown in Figure 1d,e, respectively. A 5× 5 μm PFM scan reveals local variations of the amplitude and phase of the electromechanical response of the piezoelectric material highlighting the high electroactive activity of the semi-crystalline polymer thin film (Figure S1, Supporting Information). To emphasize the thermal stability of the eSR, dielectric measurements are performed at different temperatures using a Solatron 1260 A impedance analyzer. A sinusoidal tension of 1 V amplitude between 10^2 and 10^5 Hz is applied to determine the complex relative permittivity ϵ (ϵ', ϵ'' and tan $\delta = \epsilon''/\epsilon'$) over a temperature range of 20–50 °C (Figure 1f). The relatively small variation of dielectric constant and losses as temperature increases, demonstrates that this eSR is suitable for wearable human respiratory monitoring.

The calibration of the eSR has been carried out using commercial spirometry (Smart spirometer, Spirolink), where the measurement of airflow with spirometry and the corresponding voltage produced from eSR, placed on the chest were recorded simultaneously (**Figure** 2a). Various eSRs of different thicknesses (2.5, 5.0 and 7.5 μm) of the active material layers have been fabricated to investigate the influence of the thickness on the respirometer performances. The output voltage response of these eSRs are found to increase as the thickness of the electroactive material increases. Concretely, the sensitivity shows more than two-fold enhancement and jumps from 150 to 400 mV N^{-1} with the thickness variation of P(VDF-*co*-TrFE) from 2.5 to 7.5 μm (Figure 2b). A high signal-to-noise ratio (SNR) is essential for acquiring precise signals, enabling the respirometer to extract the desired signals by eliminating the background noise. The thicker eSR exhibits a higher signal-to-noise ratio (SNR) (58 dB) (Figure 2c). Herein, 58 dB is found to be sufficient enough to detect subtle changes in breathing patterns, indicating its efficacy in capturing variations in respiratory patterns without further increasing the thickness of the active layer.[30–34] The eSR presents a high conversion factor (12 mL mV^{-1}) coupled with a low limit detection of tidal volume (100 mL) (Figure 2d), which makes it a promising respirometer wearable device even at a low value of detection. (Section S1, Supporting Information)

To equip the eSR with self-learning capabilities for COPD detection, machine learning algorithms have been integrated. Over the last years, ML-integrated sensors have revolutionized disease surveillance, offering portable, non-invasive means to continuously monitor physiological biomarkers. Among global health challenges like COVID-19, their role became crucial in curbing immediate disease spread.[35–40] In this context, **Figure** 3a outlines the step-by-step process of the self-learning eSR involved in the prediction methodology. The process workflow chart indicates the logical sequence of data acquisition, preprocessing, feature extraction, algorithm selection, model training, and breathing pattern prediction (Section S2, Supporting Information). A detailed investigation of different regression algorithms has been carried out, particularly, random forest regression (RFR), gradient boosting regression (GBR), linear regression (LR), support vector regression (SVR), and ridge regression (RR). To understand the relationship among different breathing descriptors

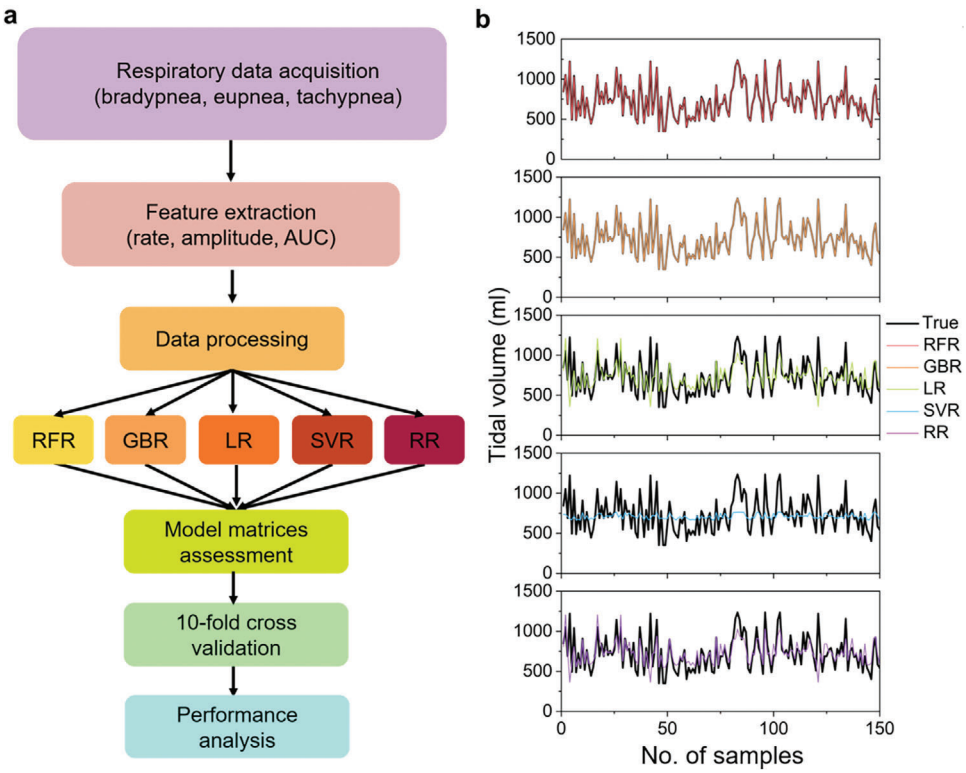

Figure 3. a) Workflow of the investigation of finding the robust algorithm for tidal volume prediction. b) True and predicted values of tidal volume for different ML algorithms.

(amplitude, area under curve (AUC) and rate), a correlation matrix has been plotted, which quantifies the strength and nature of the relationships among different descriptors (Figure S2, Supporting Information). Further visualization of the distribution of descriptors in the respiratory signals, pair plot has been utilized, providing insights into understanding the complex interactions and dependencies,[36] (Figure S3, Supporting Information). Figure 3b represents the comparison plots between the true tidal volume and predicted by different algorithms. Extensive overlapping between the true and predicted tidal volume such as for GBR and RFR indicates high-fidelity prediction in contrast to LR and RR models that exhibit medium accuracy in predictions and even SVR shows the worst prediction (Figure S4, Section S1, Supporting Information).

The consistency of the performance of these algorithms to predict tidal volume is further highlighted by comparing the Root Mean Squared Error (RMSE) values and coefficient of determination (R^2) (Figure S5, Supporting Information). **Figure** 4a displays the RMSE values obtained for each algorithm, providing a quantitative measure of the prediction accuracy. Lower RMSE values indicate higher prediction accuracy, similarly, R^2 is a statistical measure indicating the proportion of variance in the breathing pattern data. Figure 4b illustrates R^2 scores achieved by the different algorithms for tidal volume prediction. RFR presents a low RMSE of 3.47 and a high R^2 of 0.9999, indicating accurate predictions, and capturing a significant portion of variance. While GBR combines multiple weak prediction models (decision trees) sequentially by fitting new models to the residuals of previous models depicts a low RMSE of 0.2982, and a high R^2 of 0.9998, indicating its sequential model refinement leads to improved predictions. LR assumes linearity and models the relationship between input features (x_1, x_2, ..., x_i) and the target variable (y) using a linear equation, here, LR struggles with complex patterns, resulting in higher RMSE (162), and lower R^2 (0.136). SVR handles complex relationships and non-linear data by finding a hyperplane that best fits the data suboptimal performance (RMSE = 192, R^2 = 0.16913), and RR performs similarly to SVR (RMSE = 162, R^2 = 0.4070), possibly due to the linear nature limiting complex data handling.[41–43] The ten fold cross-validation is a critical validation technique that helps to evaluate the universality of the algorithm by splitting data into ten splits (folds) and iteratively using each fold as a validation set (Figure 4c). It reduces the risk of overfitting/underfitting and thus provides a more reliable and generalized performance estimation (Section S3, Supporting Information).[44,45] RMSE values of tenfold cross-validation achieved in different algorithms are displayed in Figure 4d. RFR and GBR demonstrate consistent accuracy and precision in predicting tidal volume, possessing lower RMSE, GBR standing out as the most precise. LR and SVR exhibit wider prediction error range, indicating low sensitivity to data splits and potential struggles with capturing complex patterns while RR represents moderate consistency, performing less precisely than GBR,and RFR but more stable than LR and SVR (associate discussion S4, Supporting Information).

Figure 5 displays the flow diagram of the self-learning eSR for the prediction of COPD biomarkers. Figure 5a displayed the placing of the eSR on the chest. The enlarged view (bottom) represents the cross-sectional view of eSR while the top figure shows

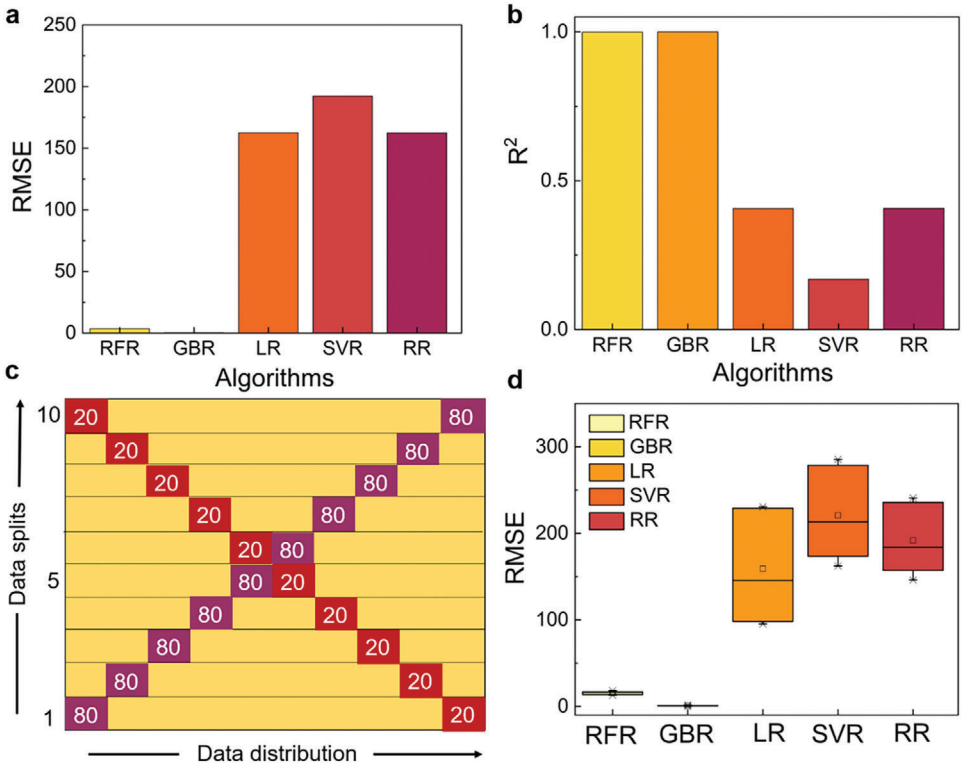

Figure 4. a) Root means square error (RMSE) and b) R2 of different investigated algorithms. c) Schematic illustration of ten-fold validation. d) RMSE values of ten-fold validation for different employed algorithms.

the acquired respiratory signals with eSR. Figure 5b presents a schematic of the machine learning (ML) model while the top enlarged view represents the mathematical equations used for mean square error (MSE), and the argument of minimum distance in the case of SVM, the bottom view shows the typical architecture of the neural network. Figure 5c shows a schematic of COPD-affected lungs, the top enlarged view represents the lung arteries affected with Emphysema, while the bottom view displays the insight structure of chronic bronchitis-affected lungs.[46,47]

To demonstrate the real-time ability of eSR for COPD biomarkers monitoring, respiratory signals for different disease conditions have been carried out using a respiratory mannequin simulator at SimBA-S healthcare platform, University of Bordeaux, France (**Figure** 6a). In particular, various COPD conditions have been simulated using the Monnal T60 healthcare signal acquisition instrument from air-liquid that allowed us to comprehensively test and validate our eSR.[48] By simulating diverse COPD conditions, we validate the reliability, and robustness of our respirometer able to record respiratory signals of different breathing conditions as shown in Figure 6b. To detect COPDs particularly emphysema and chronic bronchitis, IC and FEV1 have been selected as the key biomarkers, since these are not effectively tracked by the tidal volume measurement. For instance, in emphysema, the destruction of alveoli and loss of lung elasticity led to air trapping, dynamic hyperinflation, and increased airway resistance, resulting in a decreased inspiratory capacity.[46] This impairs the ability to efficiently inhale air, contributing to respiratory limitations, it lowers from 2600 mL in healthy conditions to 1800 mL for emphysema affected (Figure 6c). Similarly, in chronic bronchitis decreased FEV1 is primarily caused by chronic inflammation, excessive mucus production, and structural changes in the airways, leading to narrowed passages and reduced lung elasticity. It collectively impedes the smooth flow of air during forced expiration, contributing to impaired lung function, as FEV1 decreases from 90% to 42% for healthy and affected patients, respectively (Figure 6d). To early predict the different COPDs particularly emphysema and chronic bronchitis, acquired data from the disease simulator has been utilized as input in the ML model, while taking IC and FEV1 as a descriptor.[47–49] Class-wise performance has been evaluated by utilizing the Receiver Operating Characteristic (ROC) curve for each class, demonstrating the ability of the model to distinguish between the true positive rate (TPR), and false positive rate (FPR). Subsequently, our SVM classification model can distinguish between the healthy volunteers and COPD-affected patients with a classification accuracy of over 95% (Figure 6f), with a precision of 0.96 and a recall of 0.97. To test the robustness of the ML model at optimized parameters, accuracy, and loss function have been calculated with respect to different training/testing proportions (Figure S6, Supporting Information).

3. Conclusion

An organic and conformable e-skin respirometer has been demonstrated for identifying the biomarkers of progressive lung diseases through monitoring of respiratory signals. A self-learning capability has been included by the integration of ma-

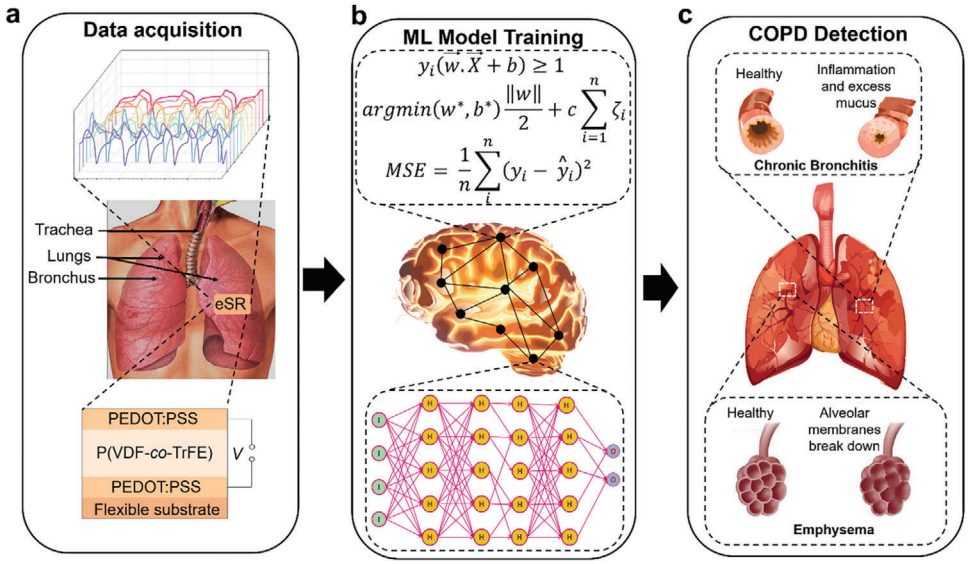

Figure 5. The process flow diagram of COPD biomarkers prediction: a) Data acquisition: eSR on the chest (center) with its cross-view structure (bottom) and enlarged view represents acquired respiratory signals (top). b) ML Model Training with the typical schematic of neural network (bottom) and the mathematical equations used (top). c) COPD detection with affected lungs (center) with zoomed view on the region of the lungs where emphysema (bottom) and chronic bronchitis (top) took place.

chine learning algorithms. Among the different algorithms investigated, GBR is found to be the most reliable one for classifying the various respiratory diseases, particularly emphysema, and chronic bronchitis with the classification exceeding 95%. In contrast to the specialized techniques, manual data recording, dedicated testing facilities, and invasive techniques, our organic self-learning eSR provides an alternative solution by allowing real-time monitoring and autonomous detection of COPDs.

4. Experimental Section

Fabrication and Characterization of the Sensor: Utilizing an Ekra X5 screen, the piezoelectric sensor underwent comprehensive screen printing for varying thicknesses (2.5, 5.0, and 7.5 µm), achieved by precise control of layer deposition during the printing process. In the initial phase, bottom electrodes were meticulously screen-printed onto a polyethylene naphthalate (PEN) substrate using a PEDOT: PSS ink (EL-P5015) procured from Agfa. The application involved a pressure of 80 N and a speed of

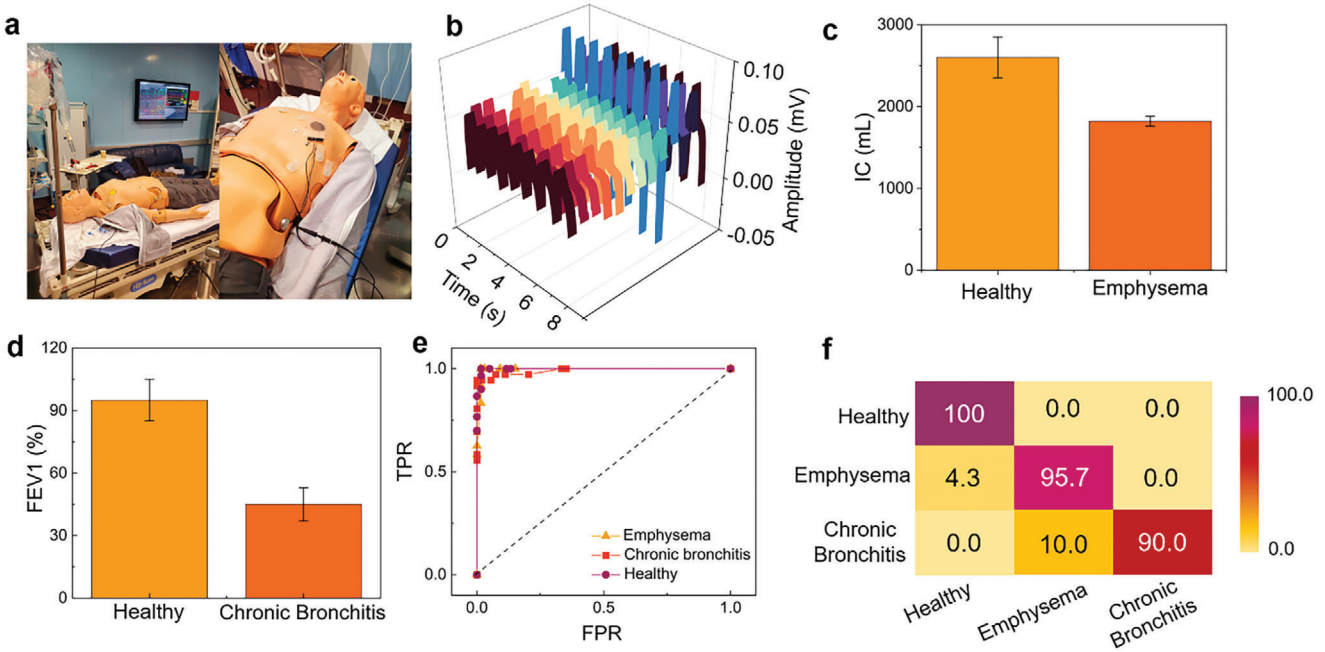

Figure 6. a) Disease simulator for different COPD disease recognition. b) recorded signal of different respiratory conditions with eSR. c) Effect on Inspiration capacity (IC) and d) forced expiration volume in 1 s. for healthy lungs and the COPD diseases affected e) ROC plot to evaluate the class wise discriminating ability of the mode f) Confusion matrix for the classification of emphysema, and chronic bronchitis.

100 mm s^{-1}, followed by annealing at 120 °C for 15 min. Subsequently, the piezoelectric semi-crystalline polymer P(VDF-*co*-TrFE) was screen-printed from a specialized piezoelectric ink (FC20 INK P) sourced from Piezotech Arkema. A dual annealing process ensured, involving steps at 80 °C for 5 min and 135 °C for 30 min immediately post-printing. Finally, mirroring the conditions employed for the bottom electrodes, the top electrodes were meticulously printed to complete the sensor assembly.

Characterization Techniques: A digital storage oscilloscope (DSOX1102G, Keysight) was used to acquire the open-circuit voltage and physiological signals. The respiratory data recording was performed on the simulator at the SimBA-S health simulation platform at Bordeaux University (Figure S7, Supporting Information).

Data Acquisition: In the non-invasive mode, all measurements were conducted, with the author assuming the role of the volunteer. Prior to data recording, explicit written consent was obtained.

Development of Machine Learning Algorithms: In the regression analysis, a diverse set of machine learning algorithms was applied to address specific tasks. RFR was employed using Python, NumPy, and Matplotlib, where the dataset underwent preprocessing, and one-hot encoding, and was split into training and testing sets. GBR utilized boosting techniques and similar preprocessing steps for evaluation. LR focused on Python, NumPy, and Matplotlib, employing one-hot encoding and visualizing the regression line. SVR utilized Python, NumPy, and Matplotlib with one-hot encoding and visualizations for assessing performance. RR was implemented using Python, NumPy, and Matplotlib, with separate X and Y data frames and one-hot encoding. Each algorithm's performance was evaluated using appropriate regression metrics and visualized to provide insights into their effectiveness in the respective tasks. Detailed information regarding each algorithm has been provided in the Section S5 (Supporting Information).

Supporting Information

Supporting Information is available from the Wiley Online Library or from the author.

Acknowledgements

This study was conducted under the auspices of the ANR JCJC DEFORM (ANR-18-CE24-0020-01) and the Raman-Charpak Fellowship (No: IFC//4141/RCF 2022/389). The authors express their gratitude to the Equipex ELORPrintTec ANR-10-EQPX-28-01 for its support in the microfabrication of the sensor. Finally, the authors would like to thank Germain Picq for the access of the SIMBA-S health simulation platform.

Conflict of Interest

The authors declare no conflict of interest.

Data Availability Statement

The data that support the findings of this study are openly available in 1 at https://github.com/ABnano/BreathInfo, reference number 1.

Keywords

COPD, digital health, e-skin, machine learning, respiratory diseases, screen printing

Received: May 22, 2024
Published online:

[1] D. H. Heck, R. Kozma, L. M. Kay, *J. Neurophysiol.* **2019**, *122*, 563.
[2] C. A. Del Negro, G. D. Funk, J. L. Feldman, *Nat. Rev. Neurosci.* **2018**, *19*, 351.
[3] I. Homma, Y. Masaoka, *Exp. Physiol.* **2008**, *93*, 1011.
[4] M. A. Matthay, R. L. Zemans, G. A. Zimmerman, Y. M. Arabi, J. R. Beitler, A. Mercat, M. Herridge, A. G. Randolph, C. S. Calfee, *Nat. Rev. Dis. Prim.* **2018**, *5*, 18.
[5] D. Chiumello, E. Carlesso, P. Cadringher, P. Caironi, F. Valenza, F. Polli, F. Tallarini, P. Cozzi, M. Cressoni, A. Colombo, J. J Marini, L. Gattinoni, *Am. J. Respir. Crit. Care Med.* **2008**, *178*, 346.
[6] J. Zhou, Y. Guo, Y. Wang, Z. Ji, Q. Zhang, F. Zhuo, J. Luo, R. Tao, J. Xie, J. Reboud, G. McHale, S. Dong, J. Luo, H. Duan, Y. Fu, *Appl. Phys. Rev.* **2023**, *10*, 021311.
[7] T. J. Barreiro, I. Perillo, *Am. Fam. Physician* **2004**, *69*, 1107.
[8] J. Wanger, J. L. Clausen, A. Coates, O. F. Pedersen, V. Brusasco, F. Burgos, R. Casaburi, R. Crapo, P. Enright, C. P. M. van der Grinten, P. Gustafsson, J. Hankinson, R. Jensen, D. Johnson, N. MacIntyre, R. McKay, M. R. Miller, D. Navajas, R. Pellegrino, G. Viegi, *Eur. Respir. J.* **2005**, *26*, 511.
[9] D. C. Mannée, F. de Jongh, H. van Helvoort, *Front. Digit. Heal.* **2020**, *2*, 559483.
[10] H. Chen, J. Zhou, X. Long, F. Zhuo, Y. Liu, Y. Zhao, J. Xie, H. Duan, Y. Fu, *Chem. Eng. J.* **2023**, *473*, 145054.
[11] H. Jin, Y. S. Abu-Raya, H. Haick, *Adv. Healthcare Mater.* **2017**, *6*, 1700024.
[12] A. Natarajan, H. W. Su, C. Heneghan, L. Blunt, C. O'Connor, L. Niehaus, *npj Digit. Med.* **2021**, *4*, 136.
[13] A. Babu, E. Raoul, G. Kassahun, I. Dufour, D. Mandal, D. Thuau, *Adv. Mater. Technol.* **2024**, *9*, 2301551.
[14] H. Chen, F. Zhuo, J. Zhou, Y. Liu, J. Zhang, S. Dong, X. Liu, A. Elmarakbi, H. Duan, Y. Fu, *Chem. Eng. J.* **2023**, *464*, 142576.
[15] Y. Yang, Y. Yuan, G. Zhang, H. Wang, Y. C. Chen, Y. Liu, C. G. Tarolli, D. Crepeau, J. Bukartyk, M. R. Junna, A. Videnovic, T. D. Ellis, M. C. Lipford, R. Dorsey, D. Katabi, *Nat. Med.* **2022**, *28*, 2207.
[16] C. Heyde, H. Mahler, K. Roecker, A. Gollhofer, *Int. J. Sports Med.* **2015**, *36*, 29.
[17] A. Nicolò, C. Massaroni, L. Passfield, *Front. Physiol.* **2017**, *8*, 992.
[18] C. G. Canning, J. A. Alison, N. E. Allen, H. Groeller, *Arch. Phys. Med. Rehabil.* **1997**, *78*, 199.
[19] D. Mereles, N. Ehlken, S. Kreuscher, S. Ghofrani, M. M. Hoeper, M. Halank, F. J. Meyer, G. Karger, J. Buss, J. Juenger, N. Holzapfel, C. Opitz, J. Winkler, F. F. J. Herth, H. Wilkens, H. A. Katus, H. Olschewski, E. Grünig, *Circulation* **2006**, *114*, 1482.
[20] L. M. Romer, M. I. Polkey, *J. Appl. Physiol.* **2008**, *104*, 879.
[21] S. A. Martin, B. D. Pence, J. A. Woods, *Exerc. Sport Sci. Rev.* **2009**, *37*, 157.
[22] M. A. Roman, H. B. Rossiter, R. Casaburi, *Eur. Respir. J.* **2016**, *48*, 1471.
[23] T. E. Dick, Y. H. Hsieh, R. R. Dhingra, D. M. Baekey, R. F. Galán, E. Wehrwein, K. F. Morris, *Prog. Brain Res.* **2014**, *209*, 191.
[24] S. H. Lee, Y. S. Kim, M. K. Yeo, M. Mahmood, N. Zavanelli, C. Chung, J. Y. Heo, Y. Kim, S. S. Jung, W. H. Yeo, *Sci. Adv.* **2022**, *8*, eabo5867.
[25] A. Zhang, L. Xing, J. Zou, J. C. Wu, *Nat. Biomed. Eng.* **2022**, *6*, 1330.
[26] L. Song, Z. Zhang, X. Xun, L. Xu, F. Gao, X. Zhao, Z. Kang, Q. Liao, Y. Zhang, *Research* **2021**, *2021*, 9801832.
[27] P. Sharma, D. Wu, S. Poddar, T. J. Reece, S. Ducharme, A. Gruverman, *J. Appl. Phys.* **2011**, *110*, 052010.
[28] A. Babu, D. Mandal, *ACS Appl. Energy Mater.* **2024**, *7*, 822.
[29] R. Roth, M. M. Koch, A. D. Rata, K. Dörr, *Adv. Electron. Mater.* **2022**, *8*, 2101416.
[30] L. Persano, C. Dagdeviren, C. Maruccio, L. De Lorenzis, D. Pisignano, *Adv. Mater.* **2014**, *26*, 7574.
[31] B. Park, J. Kim, D. Kang, C. Jeong, K. S. Kim, J. U. Kim, P. J. Yoo, T. il Kim, *Adv. Mater.* **2016**, *28*, 8130.

[32] D. E. Hurtado, J. A. P. Chavez, R. Mansilla, R. Lopez, A. Abusleme, *IEEE Access* **2020**, *8*, 227936.
[33] E. Janke, M. Zhang, S. E. Ryu, J. P. Bhattarai, M. R. Schreck, A. H. Moberly, W. Luo, L. Ding, D. W. Wesson, M. Ma, *iScience* **2022**, *25*, 105625.
[34] L. H. Mou, T. T. Han, P. E. S. Smith, E. Sharman, J. Jiang, *Adv. Sci.* **2023**, *10*, 2301020.
[35] A. K. I. Wong, P. C. Cheung, R. Kamaleswaran, G. S. Martin, A. L. Holder, *Front. Big Data* **2020**, *3*, 579774.
[36] D. Placido, B. Yuan, J. X. Hjaltelin, C. Zheng, A. D. Haue, P. J. Chmura, C. Yuan, J. Kim, R. Umeton, G. Antell, A. Chowdhury, A. Franz, L. Brais, E. Andrews, D. S. Marks, A. Regev, S. Ayandeh, M. Brophy, N. Do, P. Kraft, B. M. Wolpin, N. Fillmore, M. Rosenthal, S. Brunak, C. Sander, *Nat. Med.* **2023**, *29*, 1113.
[37] X. Wang, H. Ren, J. Ren, W. Song, Y. Qiao, Z. Ren, Y. Zhao, L. Linghu, Y. Cui, Z. Zhao, L. Chen, L. Qiu, *Comput. Methods Programs Biomed.* **2023**, *230*, 107340.
[38] L. Li, A. Ayiguli, Q. Luan, B. Yang, Y. Subinuer, H. Gong, A. Zulipikaer, J. Xu, X. Zhong, J. Ren, X. Zou, *Front. Public Heal* **2022**, *10*, 881234.
[39] J. Kaliappan, K. Srinivasan, S. Mian Qaisar, K. Sundararajan, C. Y. Chang, C. Suganthan, *Front. Public Heal* **2021**, *9*, 729795.
[40] J. Chen, K. de Hoogh, J. Gulliver, B. Hoffmann, O. Hertel, M. Ketzel, M. Bauwelinck, A. van Donkelaar, U. A. Hvidtfeldt, K. Katsouyanni, N. A. H. Janssen, R. V. Martin, E. Samoli, P. E. Schwartz, M. Stafoggia, T. Bellander, M. Strak, K. Wolf, D. Vienneau, R. Vermeulen, B. Brunekreef, G. Hoek, *Environ. Int.* **2019**, *130*, 104934.
[41] D. Chicco, M. J. Warrens, G. Jurman, *PeerJ Comput. Sci.* **2021**, *7*, e623.
[42] T. M. Dutschmann, L. Kinzel, A. ter Laak, K. Baumann, *J. Cheminform.* **2023**, *15*, 49.
[43] Y. Jung, J. Hu, *J. Nonparametr. Stat.* **2015**, *27*, 167.
[44] E. A. Kortianou, A. Aliverti, Z. Louvaris, M. Vasilopoulou, I. Nasis, A. Asimakos, S. Zakynthinos, I. Vogiatzis, *J. Appl. Physiol.* **2015**, *118*, 107.
[45] A. Babu, S. Ranpariya, D. K. Sinha, D. Mandal, *Adv. Mater. Technol.* **2023**, *8*, 2300046.
[46] S. Kim, S. K. Lee, A. Son, J.-H. Lee, H. G. Kim, *Adv. Healthcare Mater.* **2023**, *12*, 2301673.
[47] M. J. M. Cluitmans, L. R. Bear, U. C. Nguyên, B. van Rees, J. Stoks, R. M. A. ter Bekke, C. Mihl, J. Heijman, K. D. Lau, E. Vigmond, J. Bayer, C. N. W. Belterman, E. Abell, L. Labrousse, J. Rogier, O. Bernus, M. Haïssaguerre, R. J. Hassink, R. Dubois, R. Coronel, P. G. A. Volders, *Sci. Transl. Med.* **2021**, *13*, 9317.
[48] M. I. Jordan, T. M. Mitchell, *Science* **2015**, *349*, 255.
[49] A. Panesar, *Machine Learning and AI for Healthcare*, Academic Press Berkeley, CA **2019**.